analytical chemistry

pubs.acs.org/ac Article

Electrochemiluminescence of Polymer Dots Featuring Thermally Activated Delayed Fluorescence for Sensitive DNA Methylation Detection

Chao Wang, Jie Wu, Hao Huang, Qiqi Xu, and Huangxian Ju*

Cite This: https://doi.org/10.1021/acs.analchem.2c02934 Read Online

ACCESS | Metrics & More | Article Recommendations | Supporting Information

ABSTRACT: Polymer dots (Pdots) as electrochemiluminescence (ECL) emitters have drawn intensive attention for expanding the application of ECL analytical technology. Here we used a donor−acceptor polymer with thermally activated delayed fluorescence (TADF) property as a precursor to design and synthesize a kind of highly efficient Pdots with desirable annihilation and co-reactant ECL behaviors. The TADF Pdots possessed a highly stable negative-charged state in the ECL process, and their ECL emission followed the "S-route", thus achieving theoretically 100% excitons harvesting for radiative decay. With $S_2O_8^{2-}$ or tripropylamine as the co-reactant, the TADF Pdots exhibited intensive bandgap ECL emission and possessed ultrahigh ECL efficiency, which were superior to conventional fluorescent Pdots due to the TADF property and the shielding of oxygen quenching effect toward triplet excitons. By combining the stable cathodic ECL property of TADF Pdots with rolling circle amplification reaction, a sensitive ECL biosensor was designed for DNA methylation detection with RASSF1A gene fragment as a target model, which showed detection limits down to the fM level and realized the localization of the methylation site on target DNA based on steric hindrance effect. This work revealed the great potential of TADF emitters in ECL efficiency elevation and offered a new idea for the development of detection kits to quantitatively detect gene methylation.

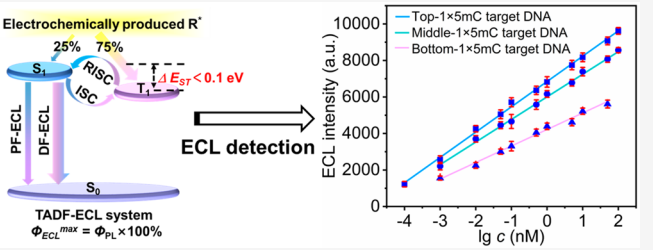

INTRODUCTION

Electrochemiluminescence (ECL) integrates the high sensitivity of chemiluminescence method with the temporal and spatial controllability of electrochemistry and has been evolved into a powerful analytical technology applied in clinical diagnosis.[1] As an attractive class of ECL emitters, polymer dots (Pdots) have mushroomed in ECL analysis due to their bright luminescence, excellent photostability, and biocompatibility.[2−7] To improve the ECL efficiency (Φ_{ECL}), our previous works designed several ECL signal amplification strategies such as electron-withdrawing group enhancement,[8] resonance energy transfer,[9] dual intramolecular resonance energy transfer,[10] aggregation induced emission,[11] and dual intramolecular electron transfer[4] by using cyanovinylene-contained PPV Pdots,[8] $Ru(bpy)_3^{2+}$ doped PFO Pdots,[9] D1−A1/D2−A2 triple-component Pdots,[10] AIE-active TPE modified D−A type Pdots,[11] and co-reactant-embedded Pdots,[4] respectively. However, the Φ_{ECL} elevation of the fluorescent Pdots is generally limited by theoretical restriction caused by spin statistics. Specifically, after the fluorescent Pdots are excited electrochemically, only the singlet (S_1) excitons (accounts for one-fourth of the total exciton number) can be radiatively decayed to generate ECL, while the remaining triplet (T_1) excitons are forbidden to transit from T_1 to ground state and fail to generate ECL. Thus, even though the photoluminescence quantum yields (Φ_{PL}) of some fluorescent Pdots are high enough, their Φ_{ECL} are still limited due to their intrinsic fluorescent properties.

To break through such a bottleneck imposed by spin statistics, this work used a thermally activated delayed fluorescence (TADF) polymer as a precursor to prepare a new kind of Pdots and realized theoretically 100% excitons harvesting for radiative decay. TADF is a phenomenon that occurs when the energy gap between S_1 and T_1 (ΔE_{ST}) is sufficiently small (ca. 0.1 eV)[12] and can achieve a high luminescent efficiency via rapid reverse intersystem crossing (RISC) of T_1 excitons to S_1 excitons to generated delayed fluorescence (DF) along with prompt fluorescence (PF).[13−15] This phenomenon has been used for the development of organic light-emitting diodes[16,17] and observed from the ECL emissions of four kinds of TADF molecules in organic media.[13,18,19] By encapsulating one of these TADF molecules in an amphiphilic shielding polymer, DSPE-PEG2000, Niu et

Received: July 7, 2022
Accepted: October 24, 2022

al. recently achieved the ECL emission of TADF emitters in aqueous media.[20] However, the Φ_{ECL} of such emitters was as low as 0.7% vs $Ru(bpy)_3^{2+}$ with the same TPrA co-reactant due to the aggregation caused quenching. More recently, the same group prepared PAPTC Pdots to achieve aqueous TADF-ECL,[21] which showed an Φ_{ECL} of 11.7% vs $Ru(bpy)_3^{2+}$ with $C_2O_4^{2-}$ as co-reactant and were thus used for the design of biosensing strategy with target dopamine quenching mechanism.

Herein, by employing ploy(TMTPA-DCB)[22] with excellent TADF property as the precursor, the TADF Pdots with high Φ_{ECL} were prepared via nanoprecipitation method (Scheme 1A). Both the annihilation and co-reactant ECL mechanisms of the TADF Pdots demonstrated their stable negative-charged state. By combining the stable cathodic ECL property of the proposed TADF Pdots with rolling circle amplification (RCA) reaction, a sensitive ECL biosensor was designed for methylation detection using the Ras-Association Domain Family 1A (RASSF1A) gene fragment as the target model (Scheme 1B). The DNA methylation of RASSF1A promoter is a frequent event in tumorigenesis especially the nasopharyngeal carcinoma, thus being recognized as a reliable biomarker in cancer diagnosis.[23,24] The methylation detection was achieved by using the DNA-functionalized TADF Pdots (Pdots-DNA) to recognize the RCA product of biotinylated oligonucleotide in situ formed on the biosensor surface, which was captured on the surface through the affinity recognition of streptavidin (SA) to biotinylated anti-5mC antibody/methylcytosine (mC) complex. The proposed ECL biosensor exhibited outstanding performance toward methylation detection with low detection limit and high specificity, providing new insights into the development of detection kits for quantitative detection of gene methylation.

Scheme 1. Schematic Diagram of (A) Preparation of Pdots-DNA, (B) Fabrication of ECL Biosensor for DNA Methylation, (C) Annihilation and Co-reactant ECL Mechanisms for TADF Pdots, and (D) Comparison of FL-ECL and TADF-ECL Systems

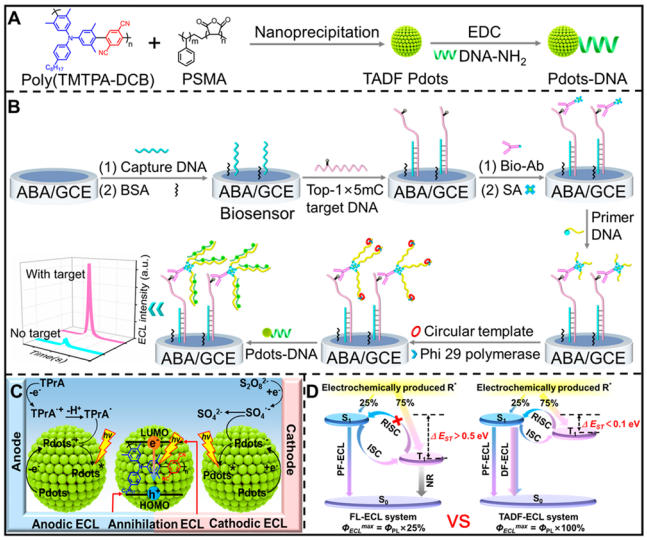

EXPERIMENTAL SECTION

Materials, Reagents, and Apparatus. The detailed information is described in the Supporting Information (SI).

Preparation of TADF Pdots and Pdots-DNA. The TADF Pdots were prepared through nanoprecipitation using poly(TMTPA-DCB) as the luminescent-conjugated polymer and poly(styrene-*co*-maleic anhydride) (PSMA) as the carboxyl-functionalized copolymer.[25] Briefly, 2.5 mL of tetrahydrofuran (THF) solution of 50 $\mu g \cdot mL^{-1}$ poly(TMTPA-DCB) and 10 $\mu g \cdot mL^{-1}$ PSMA was ultrasonically degassed for 20 min; then the solution was quickly injected into 10 mL of water and sonicated (120 W, 37 Hz) for 1 min. Afterward, the solvent THF was removed by rotary evaporation under vacuum followed by filtration through a 0.22 μm poly(ether sulfones) syringe filter to get TADF Pdots dispersion (50 $\mu g \cdot mL^{-1}$). As control, PFBT Pdots were prepared with a similar procedure.

To prepare Pdots-DNA, 6 μL of HEPES buffer (1 M) and 6 μL of PEG (5% w/v) were added to 300 μL of Pdots dispersion, and the pH was adjusted to 7.1 by adding NaOH (0.1 M). Then, 10 μL of 1-(3-(dimethylamino)propyl)-3-ethylcarbodiimide hydrochloride (EDC, 10 $mg \cdot mL^{-1}$) and 10 μL of DNA-NH_2 (100 μM) were added into the mixture and vibrated for 12 h at room temperature. To remove free DNA-NH_2, the Pdots-DNA were separated by ultrafitration for 3 times with 0.5 wt % triton X-100 in phosphate buffer saline (PBS, 0.1 M).

Preparation of Circular DNA Template. The circular DNA template was synthesized according to previous work[26] with some modifications. A 5 μL aliquot of linear DNA (100 μM), 10 μL of ligation DNA (100 μM), and 10 μL of ultrapure water were mixed and annealed at 95 °C for 5 min. After cooling to room temperature, 3 μL of T4 buffer (10×) and 2 μL of T4 DNA ligase (400 U μL^{-1}) were added to incubate at 16 °C overnight. The T4 DNA ligase was inactivated by incubation at 65 °C for 10 min. To form a circular DNA template, 5 μL of Exo I buffer (10×), 5 μL of Exo III buffer (10×), 4 μL of Exo I (20 U μL^{-1}), and 4 μL of Exo III (100 U μL^{-1}) were mixed with the above solution to react at 37 °C for 2 h. Finally, the mixture was incubated at 85 °C for 15 min to inactivate Exo I and Exo III.

Fabrication of ECL Biosensor. The glassy carbon electrode (GCE, diameter of 5 mm) was polished with 0.05 μm of alumina slurry and sonicated in ethanol and distilled water for 5 min sequentially. The cleaned electrode was electrodeposited with a layer of 4-aminobenzoic acid (ABA) according to the literature,[27] followed by modifying with 20 μL of pH 6.0 PBS containing 400 mM EDC and 100 mM *N*-hydroxysuccinimide (NHS) to activate the carboxyl group of ABA for 30 min. Then, 20 μL of capture DNA (3 μM) was covalently bound to the electrode surface by incubating at 4 °C for 10 h. The nonspecific active sites were blocked with 20 μL of bovine serum albumin (BSA, 0.25 wt %) for 40 min.

ECL Detection of DNA Methylation. After 20 μL of target DNA solution or sample with different concentrations was cast on the biosensor to hybridize with capture DNA at 37 °C for 40 min, 20 μL of bio-Ab (10 $\mu g \cdot mL^{-1}$) was added to recognize the methylation site of target DNA for 1 h. Then, 20 μL of SA (10 $\mu g \cdot mL^{-1}$) containing 0.2 wt % BSA and 100 $\mu g \cdot mL^{-1}$ salmon sperm DNA was introduced onto the electrode to bind the captured bio-Ab for 30 min. The bound SA was further incubated with 20 μL of biotinylated primer DNA (2 μM) at 37 °C for 30 min to perform the RCA reaction at 37 °C for 50 min by adding 20 μL of 10 mM pH 7.4 PBS containing 0.5 U $\cdot \mu L^{-1}$ phi 29 DNA polymerase, 200 μM dNTPs, 100 $\mu g \cdot mL^{-1}$ recombination protein, and 2 μM

https://doi.org/10.1021/acs.analchem.2c02934
Anal. Chem. XXXX, XXX, XXX−XXX

circular DNA template. After the RCA reaction was terminated by washing the electrode with 10 mM pH 7.4 PBS containing 0.05% Tween 20 (PBST), 20 μL Pdots-DNA probes were incubated on the electrode at 37 °C for 1 h to measure the ECL signal. To be noted, after each modification step, the electrode was rinsed carefully with PBST to eliminate unbound substances.

RESULTS AND DISCUSSION

Characterization of TADF Polymer and Pdots. The ploy(TMTPA-DCB) consists of triphenylamine (TPA) with two methyl groups on each side of TPA as electron donor and dicyanobenzene (DCB) as electron donor and is an almost perpendicular donor−acceptor configuration owing to the steric hindrance effect of methyl groups, enabling the effective separation between electron and hole.[22] It possesses excellent TADF property with a low ΔE_{ST} (0.0848 eV) and a long delayed fluorescence lifetime (2.29 μs).[22] The TADF Pdots prepared through the nanoprecipitation of poly(TMTPA-DCB) and PSMA exhibited spherical, monodisperse, and uniform-sized characters with an average particle size of about 10 nm (Figure 1A,B). The hydrodynamic diameter was

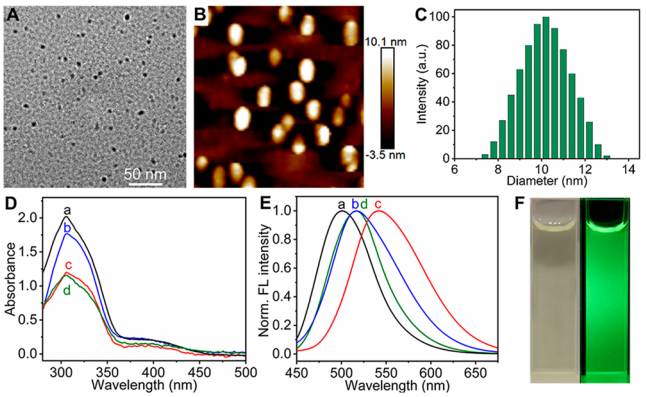

Figure 1. (A) TEM and (B) AFM images and (C) DLS characterization of TADF Pdots. (D) UV−vis absorbance and (E) FL spectra of TADF polymer in (a) MB, (b) THF, (c) DMF, and (d) TADF Pdots in water at λ_{ex} of 365 nm. (F) Photograph of TADF Pdots dispersions under daylight (left) and 365 nm irradation (right).

between 7.4 nm and 13.0 nm with an average diameter of 10.2 nm (Figure 1C). Both poly(TMTPA-DCB) and the TADF Pdots exhibited a strong UV−vis absorption at 305 nm and a weak absorption at around 400 nm in different solvents (Figure 1D), which were attributed to $\pi-\pi^*$ transition of the entire conjugated backbone and charge transfer (CT) from TPA to DCB, respectively.[28] The FL emission peak of poly(TMTPA-DCB) shifted from 500 to 542 nm, and the full width at half-maximum became wider with the increasing solvent polarity from methylbenzene (MB) to *N*,*N*-dimethylformamide (DMF) (Figure 1E) due to the CT property of D−A type polymer.[29] Meanwhile, the FL emission peak of TADF Pdots was located at 517 nm (Figure 1E, curve d), which was similar to that of poly(TMTPA-DCB) in THF (Figure 1E, curve b), demonstrating that the preparation process of Pdots exerted little influence on the FL properties of poly(TMTPA-DCB). Upon UV irradiation at 365 nm, the TADF Pdots emitted bright yellow-green light, while they were faint yellow under daylight (Figure 1F), revealing the potential of employing TADF Pdots as ECL probes.

Annihilation ECL Behaviors of TADF Pdots. The cyclic voltammograms (CV) of Pdots/GCE showed an irreversible oxidation peak at around +0.95 V and a reduction peak at around −1.72 V no matter the potential scanning direction (Figure 2A), which were related to the oxidation of TPA and

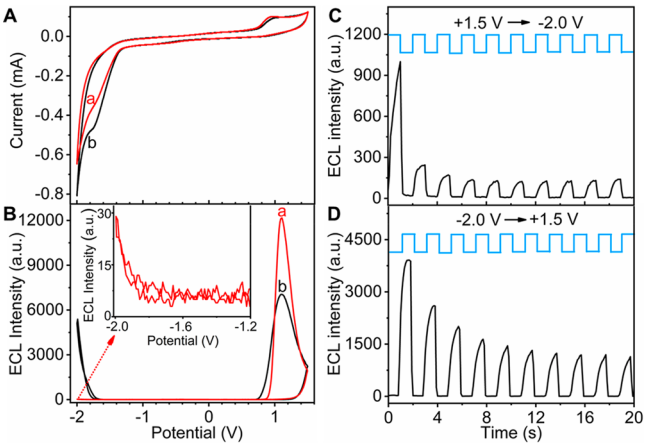

Figure 2. (A) CV and (B) ECL curves of Pdots/GCE in nitrogen-saturated 0.1 M pH 7.4 PBS (a) from 0 to +1.5 and then −2.0 V and (b) from 0 to −2.0 and then +1.5 V. (C, D) ECL transients of Pdots/GCE in nitrogen-saturated 0.1 M pH 7.4 PBS upon steps (C) from +1.5 to −2.0 V and (D) from −2.0 to +1.5 V.

the reduction of DCB, respectively.[22] However, when the CV scanning started with the cathodic direction, the reduction peak current became significantly greater (Figure 2A, curve b), indicating the production of more Pdots$^{\bullet-}$. As the potential was scanned from 0 to +1.5 and then to −2.0 V, an intense annihilation ECL peak occurred at +1.1 V along with a rather weak ECL peak at −2.0 V (Figure 2B, curve a). Contrarily, when the potential was scanned from 0 to −2.0 and then to +1.5 V, the ECL curve showed both strong cathodic and anodic responses (Figure 2B, curve b), demonstrating the excellent stability of Pdots$^{\bullet-}$.

ECL transient technology was employed to further examine the stability of radical intermediates of the Pdots. When the initial stepping potential of +1.5 V was applied, followed by stepping to −2.0 V, a relative strong ECL emission at +1.5 V was observed in the first pulse cycle, and the ECL intensity decreased dramatically in the next cycles (Figure 2C). However, when the potential of −2.0 V was applied first, the intense ECL response was not observed until the potential was switched to +1.5 V for 1 s; meanwhile, the ECL intensity decreased slowly in the subsequent pulse cycles (Figure 2D), which meant that the Pdots$^{\bullet-}$ produced first were stable enough to react with the following generated Pdots$^{\bullet+}$ for annihilation ECL emission, confirming that the reduced states of Pdots were more stable.[30,31]

Coreactant ECL Behaviors of TADF Pdots. Tripropylamine (TPrA) and $K_2S_2O_8$ were chosen as the co-reactants to study the co-reactant ECL behaviors of TADF Pdots, respectively. During the anodic process, TPrA could be oxidized to TPrA$^{\bullet+}$ (eq 1) with onset potential at +0.60 V and a peak at +0.98 V, which did not produce any ECL emission (Figure 3A,B, curves a). The Pdots/GCE showed an obvious oxidation current of Pdots (eq 2) with onset potential at about +0.90 V, and a very weak ECL signal in the absence of TPrA (Figure 3A,B, curves b) due to the presence of trace

https://doi.org/10.1021/acs.analchem.2c02934
Anal. Chem. XXXX, XXX, XXX−XXX

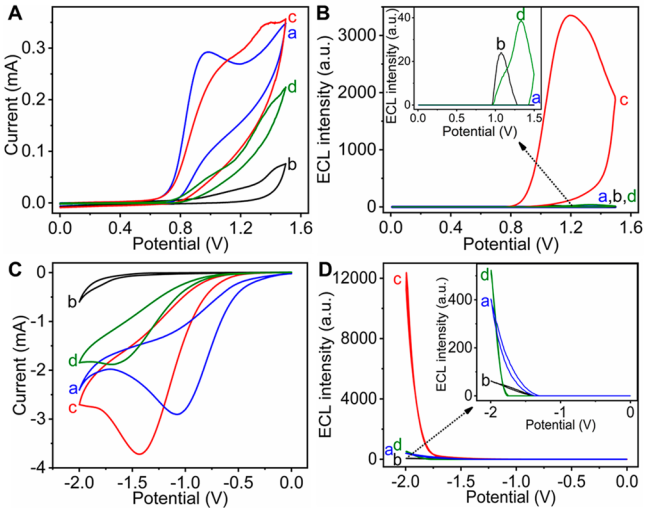

Figure 3. (A) CV and (B) ECL curves of (a) 10 mM TPrA at GCE, (b, c) Pdots/GCE in the absence (b) and presence (c) of 10 mM TPrA, and (d) polymer/GCE in 0.1 M pH 7.4 PBS containing 10 mM TPrA. (C) CV and (D) ECL curves of (a) 0.1 M $K_2S_2O_8$ at GCE, (b, c) Pdots/GCE in the absence (b) and presence (c) of 0.1 M $K_2S_2O_8$, and (d) polymer/GCE in 0.1 M pH 7.4 PBS containing 0.1 M $K_2S_2O_8$.

OH^- in PBS to serve as electron donor of produced $Pdots^{\bullet+}$.[8] In the presence of TPrA, the Pdots/GCE showed the oxidation peaks of both TPrA and Pdots (Figure 3A, curve c), and the electro-oxidation product of TPrA, $TPrA^{\bullet+}$ radical, was then deprotonated to generate $TPrA^{\bullet}$ (eq 1), which injected an electron to $Pdots^{\bullet+}$ to produce both excited singlet Pdots (^{1}Pdots*) and excited triplet Pdots (^{3}Pdots*) (eq 3), leading to strong ECL emission peak at +1.19 V (Figure 3B, curve c; Scheme 1C; eqs 4–6). Compared with Pdots/GCE, the polymer/GCE showed 85 times lower ECL emission at the same concentration of TPrA (Figure 3B, curves c,d), which could partially be attributed to less $TPrA^{\bullet+}$ formed at polymer/GCE due to the presence of a more hydrophobic polymer, which decreased the oxidation peak current of TPrA by 6 times (Figure 3A, curves c,d). More importantly, the elevated ECL emission resulted from the formation of TADF Pdots, which improved the ECL response of TADF polymer.

$$TPrA - e^- \rightarrow TPrA^{\bullet+} \rightarrow TPrA^{\bullet} + H^+ \quad (1)$$

$$Pdots - e^- \rightarrow Pdots^{\bullet+} \quad (2)$$

$$Pdots^{\bullet+} + TPrA^{\bullet} \rightarrow {}^1Pdots^*(\sim 25\%) + {}^3Pdots^*(\sim 75\%) + TPrA \quad (3)$$

$$^1Pdots^*(\sim 25\%) \rightarrow Pdots + h\nu \quad (4)$$

$$^3Pdots^*(\sim 75\%) + \Delta \rightarrow {}^1Pdots^*(\sim 75\%) \quad (5)$$

$$^1Pdots^*(\sim 75\%) \rightarrow Pdots + h\nu \quad (6)$$

In the cathodic process, $K_2S_2O_8$ showed a reduction peak around −1.06 V and a weak ECL emission at GCE due to the formation of $SO_4^{\bullet-}$ (Figure 3C,D, curves a; eq 7), while the Pdots/GCE showed a weak reduction wave and negligible ECL emission (Figure 3C,D, curves b), revealing that Pdots could be reduced electrochemically to $Pdots^{\bullet-}$ (eq 8). At the electrode surface, the formed $Pdots^{\bullet-}$ could be oxidized by the produced $SO_4^{\bullet-}$ to generate the excited ^{1}Pdots* and ^{3}Pdots* (eq 9), leading to a strong ECL emission (Figure 3D, curve c; Scheme 1C; eqs 4–6). The overlap of the reduction waves of $S_2O_8^{2-}$ with Pdots and the following chemical reaction resulted in the enhanced cathodic peak at −1.42 V (Figure 3C, curve c). Similarly, the more hydrophobic polymer modified GCE showed 24-fold lower cathodic ECL emission compared to Pdots/GCE due to the less formed $SO_4^{\bullet-}$ and the formation of TADF Pdots (Figure 3C,D, curves d).

$$S_2O_8^{2-} + e^- \rightarrow SO_4^{\bullet-} + SO_4^{2-} \quad (7)$$

$$Pdots + e^- \rightarrow Pdots^{\bullet-} \quad (8)$$

$$Pdots^{\bullet-} + SO_4^{\bullet-} \rightarrow {}^1Pdots^*(\sim 25\%) + {}^3Pdots^*(\sim 75\%) + SO_4^{2-} \quad (9)$$

ECL-Route and Efficiency of TADF Pdots. The anodic and cathodic ECL spectra of TADF Pdots both displayed the emission peaks at 520 nm, which were close to their FL emission peak at 517 nm (Supporting Information Figure S1A), demonstrating the same excited species in both ECL and FL process of TADF Pdots. The nonaqueous phase CV of Pdots/GCE was carried out to evaluate the energy level of TADF Pdots with ferrocene (Fc) as the reference (Figure S1B), and the relevant data were summarized in Table 1. The energy gap (E_g) was calculated to be 2.39 eV,[11] which was close to the optical bandgap (E_s) of 2.40 eV,[8] indicating the semiconductor character of the TADF Pdots.[30] The enthalpy ($-\Delta H$) was greater than the E_s, indicating that the energy generated from electrochemical excitation was sufficient to populate the excited singlet and triplet states.[18] Therefore, the ECL emission of the TADF Pdots followed the "S-route",[32,33] which meant that the excitons at the T_1 state could be up-converted to the S_1 state via thermal activation, thus realizing theoretically 100% excitons harvesting for radiative decay in this ECL system (Scheme 1D).

The ECL efficiencies of TADF Pdots and PFBT Pdots were compared using 1 mM $Ru(bpy)_3^{2+}$–10 mM TPrA or 0.1 M $K_2S_2O_8$ as the standard (Figure S2).[4] The relevant data were listed in Table S1. The anodic and cathodic ECL efficiencies of the TADF Pdots were 4.06 and 4.27 times higher than that of PFBT Pdots, respectively (Table 2).

Although the ECL efficiency of TADF Pdots was less than that of $Ru(bpy)_3^{2+}$ (which essentially belongs to phosphorescent luminophore), it was greatly superior to those of traditional FL Pdots (Table S2) owing to the harvest of triplet excitons for radiative decay (Scheme 1D). It is noteworthy that the cathodic ECL detection possessed better operation stability

Table 1. Summary of Key Physical Properties of TADF Pdots

λ_{PL}	λ_{ECL}	E_{ox}^{onset}	E_{red}^{onset}	E_{ox}	E_{red}	HOMO[a]	LUMO[a]	E_g[b]	E_s[c]	$-\Delta H$[d]
517 nm	520 nm	+0.99 V	−1.16 V	+1.21 V	−1.61 V	−5.48 eV	−3.09 eV	2.39 eV	2.40 eV	2.72 eV

[a]Ferrocene was used as the internal reference, and its E_{ox}^{onset} = +0.31 V, E_{red}^{onset} = +0.55 V. E_{HOMO} = -(E_{ox}^{onset}-0.31 + 4.8) eV, E_{LUMO} = -(E_{red}^{onset}-0.55+4.8) eV.[11] [b]E_g=E_{LUMO}- E_{HOMO}.[11] [c]E_s = 1239.81/λ_{PL}.[8] [d]-ΔH = E_{ox} - E_{red} - 0.1 (eV).[18]

https://doi.org/10.1021/acs.analchem.2c02934
Anal. Chem. XXXX, XXX, XXX−XXX

Table 2. ECL and PL Efficiencies of TADF Pdots and PFBT Pdots

sample	Φ_{ECL}^{nodic}[a]	$\Phi_{ECL}^{cathodic}$	Φ_{PL}	Φ_{ECL}^{max}[a]
TADF Pdots	49.9%	23.5%	73.7%	73.7%
PFBT Pdots	12.3%	5.5%	47.0%	11.75%

[a]$\Phi_{ECL}^{max} = \Phi_{PL} \times \eta$,[34] in which η is the utilization ratio of excitons. For traditional FL Pdots such as PFBT Pdots, η is equal to 25% because only the singlet excitons can be utilized, while the η value of TADF Pdots can reach 100%.

than the anodic ECL measurements (Figure S3) perhaps due to the irreversible oxidation[25] and the worse stability of $Pdots^{\bullet+}$ than $Pdots^{\bullet-}$.[30] Thus, the TADF Pdots-$K_2S_2O_8$ cathodic ECL system was applied in the subsequent ECL bioassay, though the anodic ECL efficiency was higher than the cathodic one. The theoretical maximum ECL efficiency (Φ_{ECL}^{max}) of TADF Pdots was 6.27-fold higher than that of PFBT Pdots (Table 2),[34] further proved that the TADF mechanism was beneficial to enhancing the ECL efficiency of Pdots. The Φ_{PL} of TADF Pdots was close to that of 72% for poly(TMTPA-DCB) neat film,[22] but the Φ_{PL} of poly(TMTPA-DCB) in air-saturated THF was merely 29.9%, revealing that the nanoprecipitation of TADF polymer into Pdots could avoid the oxygen quenching effect toward triplet excitons, thus enhancing the PL and ECL emission.

Construction of ECL Biosensor and Condition Optimization for DNA Methylation Detection. To verify the application of the TADF Pdots in ECL biosensing, Pdots-DNA were prepared to recognize the RCA product that was formed on the surface of biosensor after target DNA was captured and the methylation sites on target DNA were immunologically recognized (Scheme 1B). The RCA reaction was first demonstrated with electrophoretic analyses. The circular template formed using the linear DNA with the help of ligation DNA and T4 DNA ligase could hybridize with the primer DNA (Figure S4A) to trigger the RCA reaction in the presence of phi 29 DNA polymerase to produce a long DNA strand with repeated DNA sequences (Figure S4B). The Pdots-DNA was characterized with UV−vis absorption spectra and ζ-potential analysis (Figure 4A,B), which exhibited both the absorption peaks of Pdots and the typical absorption of DNA around 260 nm, and the remarkable drop of ζ-potential. After Pdots-DNA were formed, the absorption peak of DNA blue-shifted slightly due to the absorption overlap of Pdots and DNA.

Electrochemical impedance spectroscopy (EIS) was employed to examine the fabrication and detection procedures of this biosensor. To bind covalently the capture DNA to the electrode, the surface was electrodeposited with a layer of ABA,[27] which caused a great rise in electron-transfer resistance R_{et} (Figure 4C, curve b). Upon the successive assembly of capture DNA, BSA, and target DNA on the electrode, the R_{et} further increased (Figure 4C, curves c−e). The immunorecognition of bio-Ab to the methylation sites on target DNA and the following RCA reaction led to successive increases in R_{et} (Figure 4C, curves f−i). Finally, the binding of numerous Pdots-DNA to the formed long chain DNA made the R_{et} reach its maximum (Figure 4C, curve j), reflecting the successful construction of the biosensor for DNA methylation detection. The ECL responses of the biosensor were further examined under different conditions. In the absence of target DNA, the following addition of Pdots-DNA failed to generate the ECL

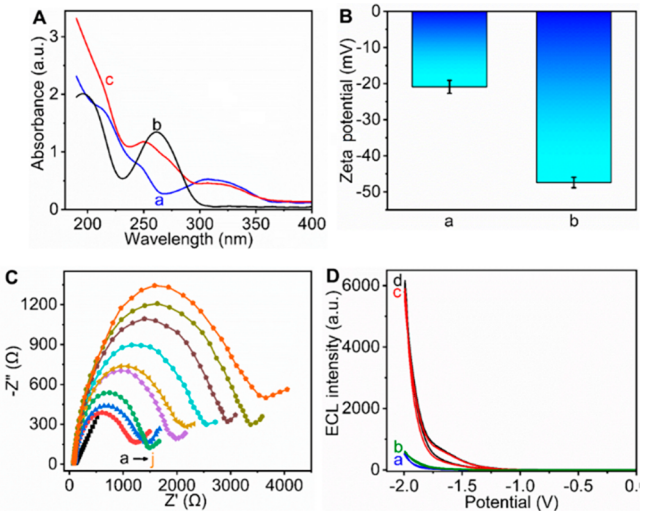

Figure 4. (A) UV−vis spectra of (a) TADF Pdots, (b) DNA-NH_2, and (c) TADF Pdots-DNA. (B) ζ-potential analysis of (a) TADF Pdots and (b) TADF Pdots-DNA. (C) EIS of (a) bare GCE and GCE assembled successively with (b) ABA, (c) capture DNA, (d) BSA, (e) target DNA, (f) bio-Ab, (g) SA, and (h) primer DNA, (i) after RCA reaction and (j) (i) after capture of TADF Pdots-DNA. (D) ECL intensity of biosensor for (a) blank and (b−d) 1 nM middle-1 × 5 mC target DNA detection in the absence (b) and presence (a, c, d) of TADF Pdots-DNA in (a, b, d) air-saturated and (c) N_2-saturated 0.1 M pH 7.4 PBS containing 0.1 M $K_2S_2O_8$.

emission (Figure 4D, curve a), probably due to the excellent inhibition effects of BSA and salmon sperm DNA toward nonspecific adsorption.[26] In the presence of target DNA, the successive assembly resulted in a strong ECL signal, while the background was negligible (Figure 4D, curves b and d), demonstrating the feasibility of this ECL sensor for DNA methylation detection. Moreover, dissolved oxygen exerted negligible influence on the ECL intensity (Figure 4D, curve c). Thus, the detection could be performed without additional deaeration.

To optimize the experimental conditions of the ECL biosensor for DNA methylation detection, the effects of pH of detection solution and concentration of co-reactant on the ECL intensity of TADF Pdots/GCE were first investigated. The TADF Pdots/GCE exhibited the strongest ECL response at pH 7.4 (Figure S5A) in the presence of 0.1 M $K_2S_2O_8$ (Figure S5B). The amount of capture DNA immobilized on the electrode was an essential factor to influence its hybridization with target DNA and the following immunorecognition and RCA reaction; hence, the concentration of capture DNA used for biosensor fabrication was optimized. At 10 nM of middle-1 × 5 mC target DNA, the ECL intensity increased with the increasing capture DNA concentration and reached a plateau at 3 μM (Figure S5C); thus 3 μM capture DNA was employed in the following biosensor fabrication. The hybridization time of capture DNA with target DNA could affect the amount of target DNA captured by the biosensor and the hybridization time was optimized to be 40 min (Figure S5D). The concentration of phi 29 polymerase and the time for RCA reaction were optimized to be 0.5 unit·μL^{-1} and 50 min, respectively (Figure S5E,F).

ECL Biosensing Performance for DNA Methylation Detection. Considering that the cytosines at different sites of DNA can be methylated, three target DNA strands with

https://doi.org/10.1021/acs.analchem.2c02934
Anal. Chem. XXXX, XXX, XXX−XXX

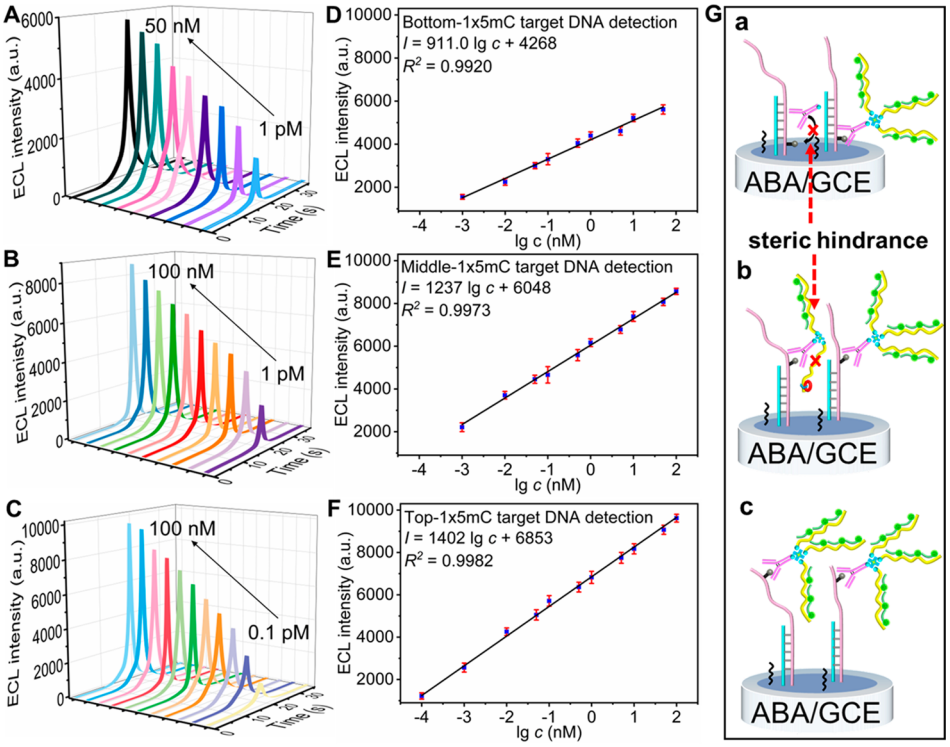

Figure 5. (A–C) ECL–time curves and (D–F) calibration curves of the biosensor for detection of (A, D) bottom-, (B, E) middle-, and (C, F) top-1 × 5 mC target DNA at different concentrations (n = 3). (G) Schematic diagram of the biosensor for detection of (a) bottom-, (b) middle-, and (c) top-1 × 5 mC target DNA.

different methylation sites were designed and named as bottom-, middle-, and top-1 × 5 mC target DNA (Table S3). Under optimal conditions, the ECL intensity increased with the increasing target DNA concentration (Figure 5A–C), and the plots of ECL intensity vs the logarithm of target DNA concentration (nM) exhibited good linearity in the concentration ranges of 1 pM to 50 nM, 1 pM to 100 nM, and 0.1 pM to 100 nM with linear equations of I = 911.0 log c + 4268 (R^2 = 0.9920), I = 1237 log c + 6048 (R^2 = 0.9973), and I = 1402 log c + 6853 (R^2 = 0.9982), and limits of detection (LODs) of 650, 300, and 60 fM at a signal-to-noise ratio of 3 for the bottom-, middle-, and top-1 × 5 mC target DNA, respectively (Figure 5D–F). The steric hindrance induced by the methylated cytosine showed obvious effect on the biosensing performance (Figure 5G), and the methylation site located at the bottom of target DNA (the hybridization zone) led to the worst sensitivity. Interestingly, the ECL response of the biosensor could be employed to distinguish bottom-, middle-, and top-1 × 5 mC target DNA (Figure S6). Taking the ECL biosensor for top-1 × 5 mC target DNA detection as an example, its detection performance was comparable and even superior to other methods (Table S4) due to the specific immunorecognition and effective signal amplification.

Using the middle-1 × 5 mC target DNA as the target model, the biosensor showed superb operation stability under continuous cyclic scanning and acceptable storage stability as the ECL intensity still remained 81.5% of its initial value after storage for 4 weeks (Figure S7A,B). The specificity of the biosensor was evaluated via using the same target DNA without methylation site (0 × 5 mC target DNA) and other DNA strands with 7 methylation sites (7 × 5mC PCDHGB7) as the interferents. The results showed that the biosensor possessed high specificity toward the middle-1 × 5 mC target DNA (Figure S7C). Meanwhile, the biosensor exhibited excellent reproducibility as the relative standard deviations (RSDs) for both intra- and interassay were within 3.0% (Figure S7D).

Real Sample Analysis. Recovery experiments were conducted to test the accuracy of the biosensor for DNA methylation detection via adding 0.05 M, 0.5 M, 5.0 M, and 50 nM of middle-1 × 5 mC target DNA into human serum samples. The recoveries were calculated to be 84.0%, 88.0%, 102%, and 90.4% with RSDs of 3.9%, 2.7%, 2.3%, and 4.1%, respectively (Table S5), revealing the acceptable reliability of this protocol for DNA methylation detection and good specificity of the biosensor even in complex matrix. Compared with the commercial RASSF1A gene methylation detection kit which could only provide qualitative information, the proposed biosensor could quantitatively detect the methylation of RASSF1A gene in a bisulfite-treatment-free and PCR-free manner, and thus might be useful in judgment of tumor subclassification, prognosis, and prediction of treatment effect. However, the proposed biosensor could only detect the methylation of target DNA with specific DNA sequence, which might limit its application in real sample analysis.

CONCLUSION

A donor–acceptor type polymer containing triphenylamine and dicyanobenzene has been used as the luminescent precursor to prepare highly efficient Pdots with TADF property. The TADF Pdots show excellent annihilation and co-reactant ECL behaviors, which demonstrate the stable negative-charged state and can harvest theoretically 100% excitons for ECL emission following the "S-route". Due to the TADF property and the shielding of oxygen quenching effect toward triplet excitons, the TADF Pdots exhibit ultrahigh ECL

https://doi.org/10.1021/acs.analchem.2c02934
Anal. Chem. XXXX, XXX, XXX–XXX

efficiency in the presence of co-reactants, which is superior to conventional fluorescent Pdots. Taking the advantages of the stable cathodic ECL emission, a sensitive ECL biosensing strategy for DNA methylation detection has been designed using the TADF Pdots-DNA as nanoprobe and the RCA reaction for signal amplification. Using methylated RASSF1A gene fragment as analyte, the proposed method shows excellent specificity, high sensitivity, good stability, and acceptable reliability and can distinguish the location of the methylation site on target DNA. The TADF Pdots with high ECL efficiency and the cathodic ECL application of TADF Pdots in methylation detection with excellent performances indicate the great potential of TADF Pdots in ECL efficiency improvement and bioanalytical application.

■ ASSOCIATED CONTENT

Supporting Information

The Supporting Information is available free of charge at https://pubs.acs.org/doi/10.1021/acs.analchem.2c02934.

Materials and reagents, apparatus, ECL and PL spectra, CV and ECL intensity−time curves, gel electrophoresis images, UV−vis and ζ-potential, EIS and ECL biosensor characterizations, optimization of experimental conditions, ECL biosensor intensity and performance, relative ECL efficiency calculation, comparison of ECL efficiencies, DNA sequences, performance comparison, and real sample analysis (PDF)

■ AUTHOR INFORMATION

Corresponding Author

Huangxian Ju − *State Key Laboratory of Analytical Chemistry for Life Science, School of Chemistry and Chemical Engineering, Nanjing University, Nanjing 210023, China;* orcid.org/0000-0002-6741-5302; Email: hxju@nju.edu.cn; Fax: +86-25-89683593

Authors

Chao Wang − *State Key Laboratory of Analytical Chemistry for Life Science, School of Chemistry and Chemical Engineering, Nanjing University, Nanjing 210023, China*

Jie Wu − *State Key Laboratory of Analytical Chemistry for Life Science, School of Chemistry and Chemical Engineering, Nanjing University, Nanjing 210023, China;* orcid.org/0000-0003-1379-122X

Hao Huang − *Research & Development Center, Canon Medical Systems (China) Co., Ltd., Beijing 100015, China*

Qiqi Xu − *Research & Development Center, Canon Medical Systems (China) Co., Ltd., Beijing 100015, China*

Complete contact information is available at: https://pubs.acs.org/10.1021/acs.analchem.2c02934

Notes

The authors declare no competing financial interest.

■ ACKNOWLEDGMENTS

This work was financially supported by the National Natural Science Foundation of China (21890741, 21827812), the Canon Medical Systems Corp. (2021200858), and the Science and Technology Project of Nanjing City (202110023).

■ REFERENCES

(1) Hu, L. Z.; Xu, G. B. *Chem. Soc. Rev.* **2010**, *39*, 3275−3304.
(2) Luo, J. H.; Li, Q.; Chen, S. H.; Yuan, R. *ACS Appl. Mater. Interfaces* **2019**, *11*, 27363−27370.
(3) Wang, Z. Y.; Pan, J. B.; Li, Q.; Zhou, Y.; Yang, S.; Xu, J. J.; Hua, D. B. *Adv. Funct. Mater.* **2020**, *30*, 2000220.
(4) Wang, N. N.; Gao, H.; Li, Y. Z.; Li, G. M.; Chen, W. W.; Jin, Z. C.; Lei, J. P.; Wei, Q.; Ju, H. X. *Angew. Chem., Int. Ed.* **2021**, *60*, 197−201.
(5) Chang, Y. L.; Palacios, R. E.; Fan, F. F.; Bard, A. J.; Barbara, P. F. *J. Am. Chem. Soc.* **2008**, *130*, 8906−8907.
(6) Zhang, N.; Gao, H.; Jia, Y. L.; Pan, J. B.; Luo, X. L.; Chen, H. Y.; Xu, J. J. *Anal. Chem.* **2021**, *93*, 6857−6864.
(7) Chen, Y. Y.; He, Y.; Zhao, J. W.; Zhang, J.; Yuan, R.; Chen, S. H. *Anal. Chem.* **2022**, *94*, 4446−4454.
(8) Feng, Y. Q.; Wang, N. N.; Ju, H. X. *Anal. Chem.* **2018**, *90*, 1202−1208.
(9) Feng, Y. Q.; Sun, F.; Wang, N. N.; Lei, J. P.; Ju, H. X. *Anal. Chem.* **2017**, *89*, 7659−7666.
(10) Wang, N. N.; Wang, Z. Y.; Chen, L. Z.; Chen, W. W.; Quan, Y. W.; Cheng, Y. X.; Ju, H. X. *Chem. Sci.* **2019**, *10*, 6815−6820.
(11) Wang, Z. Y.; Wang, N. N.; Gao, H.; Quan, Y. W.; Ju, H. X.; Cheng, Y. X. *Analyst* **2020**, *145*, 233−239.
(12) Youn Lee, S.; Yasuda, T.; Nomura, H.; Adachi, C. *Appl. Phys. Lett.* **2012**, *101*, 093306.
(13) Ishimatsu, R.; Matsunami, S.; Kasahara, T.; Mizuno, J.; Edura, T.; Adachi, C.; Nakano, K.; Imato, T. *Angew. Chem., Int. Ed.* **2014**, *53*, 6993−6996.
(14) Liu, Y. C.; Li, C. S.; Ren, Z. J.; Yan, S. K.; Bryce, M. R. *Nat. Rev. Mater.* **2018**, *3*, 18020.
(15) Uoyama, H.; Goushi, K.; Shizu, K.; Nomura, H.; Adachi, C. *Nature* **2012**, *492*, 234−238.
(16) Nakagawa, T.; Ku, S. Y.; Wong, K. T.; Adachi, C. *Chem. Commun.* **2012**, *48*, 9580−9582.
(17) Dias, F. B.; Bourdakos, K. N.; Jankus, V.; Moss, K. C.; Kamtekar, K. T.; Bhalla, V.; Santos, J.; Bryce, M. R.; Monkman, A. P. *Adv. Mater.* **2013**, *25*, 3707−3714.
(18) Kumar, S.; Tourneur, P.; Adsetts, J. R.; Wong, M. Y.; Rajamalli, P.; Chen, D. Y.; Lazzaroni, R.; Viville, P.; Cordes, D. B.; Slawin, A. M. Z.; Olivier, Y.; Cornil, J.; Ding, Z. F.; Zysman-Colman, E. *J. Mater. Chem. C* **2022**, *10*, 4646−4667.
(19) Ishimatsu, R.; Edura, T.; Adachi, C.; Nakano, K.; Imato, T. *Chem.—Eur. J.* **2016**, *22*, 4889−4898.
(20) Zeng, Z. H.; Huang, P.; Kong, Y.; Tong, L. P.; Zhang, B. H.; Luo, Y. L.; Chen, L. J.; Zhang, Y. W.; Han, D. X.; Niu, L. *Chem. Commun.* **2021**, *57*, 5262−5265.
(21) Luo, Y. L.; Zhao, B. L.; Zhang, B. H.; Lan, Y. Y.; Chen, L. J.; Zhang, Y. W.; Bao, Y.; Niu, L. *Analyst* **2022**, *147*, 2442−2451.
(22) Rao, J. C.; Yang, L. Q.; Li, X.; Zhao, L.; Wang, S. M.; Tian, H. K.; Ding, J. Q.; Wang, L. X. *Angew. Chem., Int. Ed.* **2021**, *60*, 9635−9641.
(23) Richter, A. M.; Pfeifer, G. P.; Dammann, R. H. *Biochim. Biophys. Acta, Rev. Cancer.* **2009**, *1796*, 114−128.
(24) Cao, A. P.; Zhang, C. Y. *Anal. Chem.* **2012**, *84*, 6199−6205.
(25) Feng, Y. Q.; Dai, C. H.; Lei, J. P.; Ju, H. X.; Cheng, Y. X. *Anal. Chem.* **2016**, *88*, 845−850.
(26) Cheng, W.; Yan, F.; Ding, L.; Ju, H. X.; Yin, Y. B. *Anal. Chem.* **2010**, *82*, 3337−3342.
(27) Zhou, J.; Nie, L.; Zhang, B.; Zou, G. Z. *Anal. Chem.* **2018**, *90*, 12361−12365.
(28) Rao, J. C.; Yang, L. Q.; Li, X. F.; Zhao, L.; Wang, S. M.; Ding, J. Q.; Wang, L. X. *Angew. Chem., Int. Ed.* **2020**, *59*, 17903−17909.
(29) Rizzo, F.; Polo, F.; Bottaro, G.; Fantacci, S.; Antonello, S.; Armelao, L.; Quici, S.; Maran, F. *J. Am. Chem. Soc.* **2017**, *139*, 2060−2069.
(30) Jin, Z. C.; Zhu, X. R.; Wang, N. N.; Li, Y. F.; Ju, H. X.; Lei, J. P. *Angew. Chem., Int. Ed.* **2020**, *59*, 10446−10450.
(31) Yan, M. X.; Xin, J. H.; Fan, L. B.; Ye, J.; Xiao, T.; Huang, J. S.; Yang, X. R. *Anal. Chem.* **2021**, *93*, 3461−3469.
(32) Polo, F.; Rizzo, F.; Veiga-Gutierrez, M.; De Cola, L.; Quici, S. *J. Am. Chem. Soc.* **2012**, *134*, 15402−15409.

(33) Miao, W. J. *Chem. Rev.* **2008**, *108*, 2506−2553.
(34) Huang, P.; Zhang, B. H.; Hu, Q.; Zhao, B. L.; Zhu, Y. H.; Zhang, Y. W.; Kong, Y.; Zeng, Z. H.; Bao, Y.; Wang, W.; Cheng, Y. X.; Niu, L. *ChemPhysChem* **2021**, *22*, 726−732.

https://doi.org/10.1021/acs.analchem.2c02934
Anal. Chem. XXXX, XXX, XXX−XXX